Contact line hydrodynamics with SPH

S. Adami, X.Y. Hu, N.A. Adams
Institute of Aerodynamics and Fluid Mechanics
Technische Universität München
Garching, Germany
stefan.adami@tum.de

***Abstract*—Surface tension effects can dominate multi-phase flows when the length scales of the problem are small. The resulting Capillary forces at a phase interface between two immiscible fluids are proportional to the local curvature of the flow and try to minimize the interfacial area. A more complex situation occurs when three phases are in contact or when two phases are in contact with a wall. The simulation of the contact line at a wall is still a challenging task since the motion of the contact line is contradictory to the no-slip assumption at walls.**

In this work we present a multi-phase SPH method considering surface tension effects that is capable of simulating contact line problems. Based on previous works [4] we revisit our finite-width interface model and introduce a new stress boundary condition at the wall.

I. Introduction

SPH [5] offers a powerful framework to model complex multi-phase phenomena due to its Lagrangian formulation. Using particles as discretization points and advecting them with the flow it is straightforward to introduce multiple types of particles of different phases and include phase interactions such as surface tension forces. By the nature of the method no interface capturing is required and the method is mass and momentum conservative (note, we use the mass conserving density summation form).

Morris [6] proposed a multi-phase SPH model based on the continuum surface force model (CSF) [1] to account for surface tension effects. He applied this model to isolated drops and analysed capillary waves. But this method does not conserve momentum and the calculation of the curvature is cumbersome.

Another approach to model the surface-tension effects on a macroscopic scale without the need of calculating the curvature is presented in Hu and Adams [4]. There, a stress tensor is calculated from the color-index gradients and the resulting surface tension forces conserve linear momentum. They showed that this method captures the dynamics of isolated drops in shear flows and presented a three-phase interaction with triple junction. Fundamentally different, Nugent and Posch [8] model the surface-tension effect with microscopic inter-phase attractive potentials. This method is appealing since simple pair-wise interactions are introduced without the need of a color-index gradient calculation. But on the other hand the remaining parameter in the model have to be calibrated as there is no analytical relation between the resulting surface tension coefficient and the model parameter. Tartakovsky and Meaking [9] proposed a similar method and studied the influence of contact angles on flows through bifurcations. Recently, Das and Das [2] used SPH to simulate equilibrium shapes and contact angles of sessile drops. They used a CSF model and adjusted the position of the wall-nearest SPH particles according to the static contact angle as found from the Young-Laplace equation to impose the equilibrium contact angle. Furthermore they showed that their results could be improved with a diffuse-interface approximation. But consequently, the thickness of the transition region along the interface is doubled and it is not clear how this method performs in dynamic situations since static equilibrium angles are imposed at the contact line.

In this work we propose an extension of the original method of Hu and Adams [4] to simulate contact angle problems. Using the original formulation to simulate the equilibrium contact angle and shape of a drop on a flat surface we achieved already physically reasonable results. That means the wetting or non-wetting behaviour of the fluid on the wall was represented correctly according to the surface-tension coefficients. But analysing the equilibrium state we found comparably strong spurious currents close to the triple point (in two dimensions the triple line or contact line reduce to a triple point or contact point, respectively), see Fig. 1.

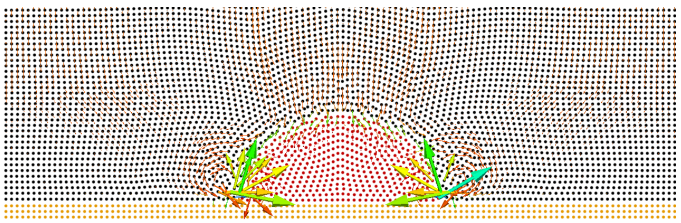

Fig. 1. Velocity vectors showing spurious currents at triple point.

Particles close the triple line are continuously accelerated since the stress singularity is not discretized correctly and consequently the kinetic energy does not decrease. To solve this problem we introduced a new stress boundary condition at the wall that requires only a simple extrapolation of the nearest adjacent phase. Then, the stress at an interface particle is calculated based on its real neighbour particles and its interpolated image particles. With this new approach we are

able to decrease the kinetic energy in the equilibrium system by almost three orders of magnitude.

II. Governing equations

In our multi-phase SPH model we use the mass conserving density summation form

$$\rho_i = m_i \sum_j W_{ij} \tag{1}$$

to calculate the density of a particle i during the simulation. Following the weakly-compressible approach we introduce an equation-of-state to relate the pressure to the density

$$p = p_0 \left[\left(\frac{\rho}{\rho_0} \right)^\gamma - 1 \right] + \chi \ , \tag{2}$$

where p_0 and χ are the reference pressure and background pressure, respectively. When simulating fluids we use the exponent $\gamma = 7$. The background pressure is required in our surface-tension model to avoid negative pressures that might occur due to the pressure drop at the phase interface. The acceleration of each particle follows from the incompressible Navier-Stokes equation

$$\frac{d\vec{\mathbf{v}}}{dt} = \vec{\mathbf{g}} + \frac{1}{\rho} \left(-\nabla p + \eta \Delta \vec{\mathbf{v}} + \mathbf{F}^{(s)} \right) \ , \tag{3}$$

where $\vec{\mathbf{g}}$ is the body force, η the dynamic viscosity and $\mathbf{F}^{(s)}$ the surface tension force. For each phase we define a color index C that is equal to one if a particle belongs to this phase and zero otherwise

$$C_i^s = \begin{cases} 1, & \text{if particle i belongs to phase s} \\ 0, & \text{else.} \end{cases} \tag{4}$$

For each particle i of phase k we can then calculate the gradient of the color-index function for the interface $k - l$ using all neighbouring particles j that belong to the phase l

$$\nabla C_i^{kl} = \frac{1}{V_i} \sum_j \left(V_i^2 C_i^l + V_j^2 C_j^l \right) \nabla W_{ij} \ , \quad l \neq k \ . \tag{5}$$

Using the normalized color-index gradient as normal direction at the interface and $\left| \nabla C^{kl} \right|$ as approximation of the surface-delta function between the phases k and l the interfacial stress tensor Π is obtained from

$$\Pi = \sum_l \alpha^{kl} \left(\frac{1}{d} \mathbf{I} \left| \nabla C^{kl} \right|^2 - \nabla C^{kl} \nabla C^{kl} \right), \quad l \neq k \ . \tag{6}$$

This stress tensor is used in the continuum surface stress (CSS) model to calculate the surface tension force

$$\mathbf{F}^{(s)} = \nabla \cdot \Pi \ . \tag{7}$$

The pressure and viscous term in the Navier-Stokes equation are discretized using a standard SPH approximation, see [4] for the details. The magnitude of the sound speed, reference pressure and the timestep criteria are chosen according to Morris et al. [7] in order to limit the density variation in the system to an admissible level. For the smoothing kernel we use a quintic spline function with a cutoff of $r_c = 3h$ and the smoothing length h is equal to the initial particle distance Δx. We evolve the governing equations for the fluid particles in time using a velocity-verlet timestepping scheme.

III. Contact line discretization

We consider a three-phase contact line problem as shown in Fig. 2(a). The two liquid phases and the solid wall phase are represented by the bold markers $+$, $\mathbf{\Delta}$ and $\bigcirc$, respectively. This setup produces comparably strong spurious currents close to the triple line because the force balance for interface particles at the wall is not in equilibrium. We propose to mimick a symmetry boundary condition at the wall for the surface stress that resolves this imbalance. Therefore we extrapolate the phase type of each particle to its nearest neighbor of different type, see Fig. 2(b) for the image phase types of the particles. Although this procedure does not reproduce exactly

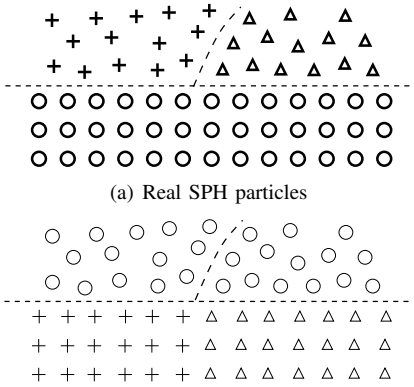

(a) Real SPH particles

(b) Extrapolated image phase types at the real particle positions.

Fig. 2. Schematic view of a contact line problem with three different types of particles ($\bigcirc$: wall particles, $+$: fluid '1', $\mathbf{\Delta}$: fluid '2')

a symmetry condition, it is very simple and applicable to arbitrarily shaped fluid-solid interfaces. In the surface tension model we now simply include also the phase interactions between real particles and particles where the image phase type is different, e.g. interactions between fluid particles of type $+$ and solid particles with the image type '$\mathbf{\Delta}$' are included when calculating the color-index gradient between the two phases $+$ and $\mathbf{\Delta}$.

IV. Numerical examples

In this section we show several test cases of the modified multi-phase model that demonstrate the improvement of the scheme regarding the decrease of the spurious motion close the triple point. At first, we place a rectangular patch of fluid on a flat surface and look at the equilibrium contact angle after a circular drop has developed. The second case shows the spreading effect of a drop due to gravity.

A. *Static contact angle*

We consider the evolution of a rectangular patch of fluid on a flat wall and monitor the shape and kinetic energy over time. In the absence of gravity the final contact angle θ between the three-phase line is given by the Young-Laplace law

$$cos\ \theta = \frac{\sigma^{1w} - \sigma^{2w}}{\sigma^{12}} \ . \tag{8}$$

Here, σ^{1w} and σ^{2w} denote the surface tension coefficient between the fluid phases '1' and '2' and the solid wall phase 'w'. The fluid-fluid coefficient is given by σ^{12}. As a reference, we simulate the drop on a wall with the original method [4] and set the wall-interaction to zero, i.e. σ^{1w} and σ^{2w} are both equal to zero. The drop liquid is initially placed in a rectangular box of size $L_x = 1$ and $L_y = 0.5$ and we set the surface tension to $\sigma^{12} = 1$. The initial particle distance is $3\Delta x = 0.1$, thus a total of 450 particles is used to discretize the bubble phase. Due to surface-tension effects the interfacial energy is minimized and a circular cap shape develops. Fig. 3 shows a snapshot at T=5 of the particles colored with the phase index. Additionally, velocity vectors show the instantaneous motion of the particles. In agreement with theory the surface

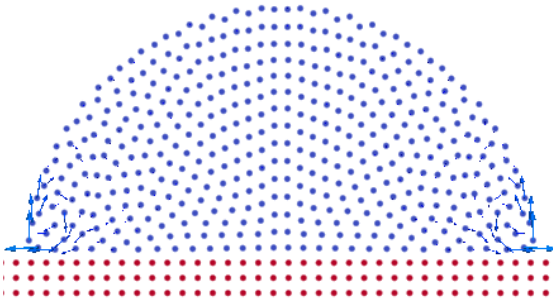

Fig. 3. Reference result using the original method [4]: snapshot of drop particles (blue) and solid wall particles (red) with velocity vectors showing the instantaneous velocity field.

stress at the triple point leads to a contact angle of $\theta = 90°$. But there occurs a non-vanishing spurious motion close to the three-phase interface. Looking at the color-index gradients at these particles it occurs that due to the lack of fluid particles on the solid side the effective fluid interface is not perpendicular to the wall. Consequently, the divergence of the stress tensor results also in a tangential force component that continuously accelerates fluid particles towards the contact point and induce these small vortices.

The result of this simulation using our new approach is shown in Fig. 4. Again, the contact angle between the drop and the surrounding phase at the wall is $\theta = 90°$. But now the vortices close the wall disappeared and a steady particle configuration is achieved. In Fig. 5 we compare the kinetic energy of the drop phase for the reference simulation and the new result. The red curve denotes the temporal evolution of the reference case. Initially, particles settle to the macroscopic

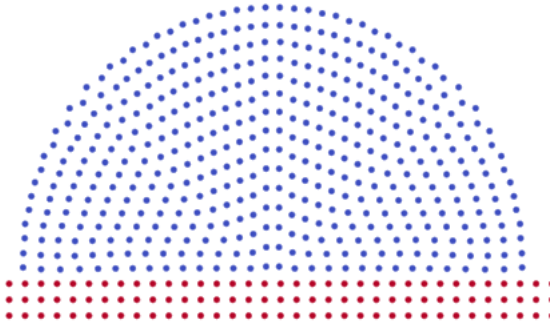

Fig. 4. Snapshot of drop particles (blue) and solid wall particles (red) with velocity vectors showing the instantaneous velocity field using our new approach.

equilibrium shape and the kinetic energy decreases. After this transient period the drop shape does not change anymore and the spurious vortices keep the kinetic energy at an almost constant level. Contrarily, the blue curve shows the result for the same case but using our modified multi-phase model. At early times up to $T \approx 5$ the two curves almost match. Then, due to the balanced surface-stress condition at the triple point the system tends to reach a global equilibrium state and the kinetic energy decreases. We compared this result with the decay of the kinetic energy of a pure drop in an ambient phase when using one symmetry at the drop center, see the black curve in Fig. 5. This case is equivalent to the drop on a wall where the wall surface-tension coefficients are zero. The energy evolution shows a very similar tendency and the absolute energy level differs by about three orders of magnitude compared to the original method.

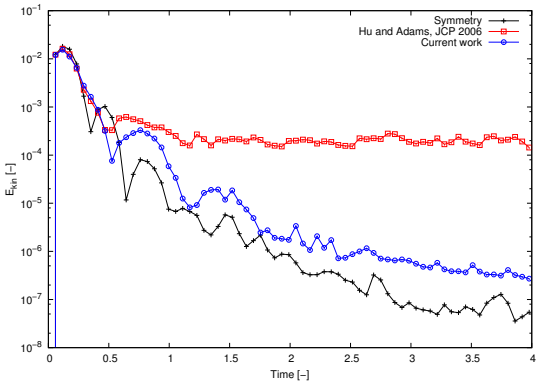

Fig. 5. Comparison of the kinetic energy for the drop on a solid wall with $\theta = 90°$.

In the following we briefly demonstrate the validity of our method for non-zero wall surface stresses. Exemplarily we show two cases for a wetting and a non-wetting wall. In the first case, the surface-tension coefficients are $\sigma^{12} = 1$, $\sigma^{1w} = 1$ and $\sigma^{2w} = 0.5$. Here, phase '1' denotes the droplet phase and '2' the continuous matrix phase. Due to the different wall surface stresses the drop phase exhibits

non-wetting behaviour and a contact angle larger than $90°$ develops. Conversely, exchanging the parameter for the wall surface stress gives a wetting surface that results in a contact angle smaller than $90°$. Fig. 6 shows a particle snapshot for the two cases. A simple estimation of the contact angle using the wall closest interface particles agree with the Young-Laplace law within an error of 5%.

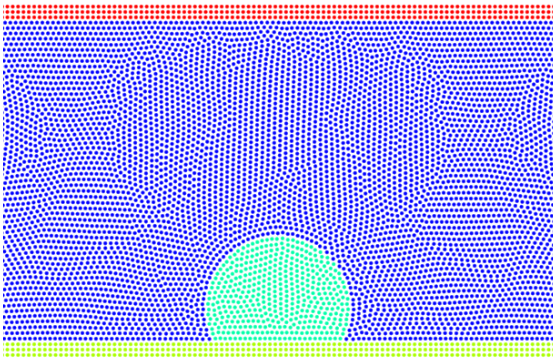

(a) Particle snapshot for the non-wetting example ($\sigma^{12} = 1$, $\sigma^{1w} = 1$ and $\sigma^{2w} = 0.5$).

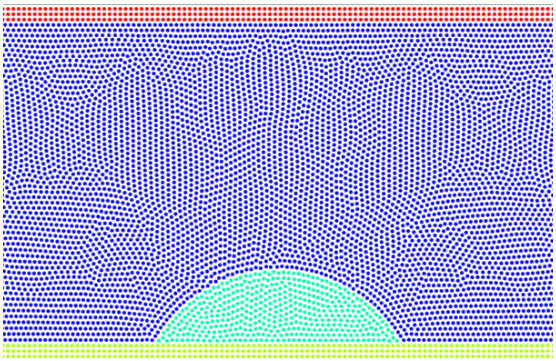

(b) Particle snapshot for the wetting example ($\sigma^{12} = 1$, $\sigma^{1w} = 0.5$ and $\sigma^{2w} = 1$).

Fig. 6. results

B. *Spreading effect due to gravity*

We place a semicircle drop on a flat wall with initial contact angle of $\theta_S = 90°$. Due to gravity the drop flattens while maintaining the contact angle with the wall. A measure for the effect of the gravity is the Eotvos number

$$Eo = \frac{\rho_L g R_0^2}{\sigma} \ , \tag{9}$$

that relates the surface tension force to the gravitational force. Here, ρ_L and R_0^2 denote the reference density of the liquid and the radius of the initial drop circle, respectively. For small Eotvos numbers (Eo $\ll 1$) the surface tension dominates the problem and the shape of the drop is a circular cap with the contact angle θ_s. In this regime the height of the drop is obtained by

$$e_0 = R_0 \left(1 - \cos\theta_s\right) \sqrt{\frac{\pi}{2\left(\theta_s - \sin\theta_s \ \cos\theta_s\right)}} \ . \tag{10}$$

With increasing influence of gravity (Eo $\gg 1$) the thickness of the liquid is proportional to the capillary length

$$e_\infty = 2\sqrt{\frac{\sigma}{\rho_L g}} \sin\left(\frac{\theta_s}{2}\right) \ . \tag{11}$$

We simulated this problem for Eotvos numbers in the range of 0.001 to 20. The semicircular drop with initial radius of $R_0 = 1$ is discretized with liquid particles with an initial particle distance of $3\Delta x = 0.1$ and the size of the surrounding channel is $L_x = 8$ $L_y = 2$. The surface tension coefficients between the fluids and the wall are all set to one, thus the static contact angle is $\theta_s = 90°$. Fig. 7 shows the non-dimensional height of the drop e/e_0 for increasing Eotvos number. Also, the two dashed curves show the two regimes of surface tension dominated spreading (eq. (10)) and gravity dominated spreading of a drop on a wall (eq. (11)). Our simulation results agree well with the asymptotic solutions and are comparable to the results of Dupont et al. [3], who simulated this case using a volume-of-fluid method.

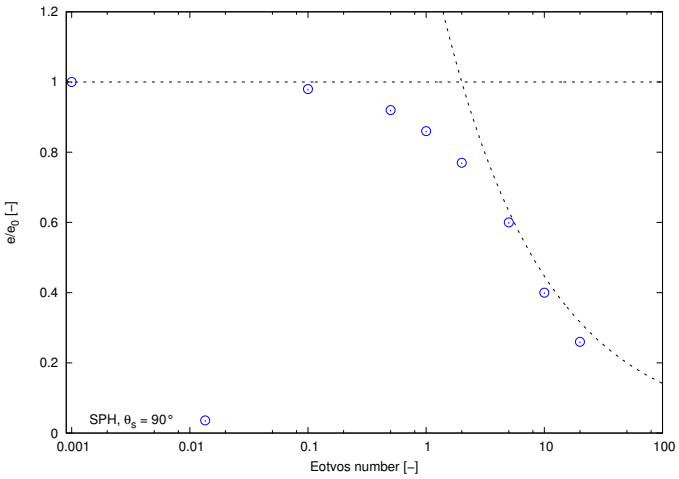

Fig. 7. Influence of the Eotvos number on the non-dimensional thickness $e = e/e_0$ of a drop on a wall.

Figs. 8-10 show exemplary the final equilibrium shape of the settled drop for $Eo = 0$, $Eo = 2$ and $Eo = 20$. Without gravity ($Eo = 0$), the semicircular drop maintains its initial shape and the non-dimensional height of the drop is $e = 1$. With increasing body force the drop spreads on the wall and its circular shape flattens. The phase interface at the contact line moves outwards due to the liquid settling under gravity and reaches the new steady state while preserving the initial contact angle.

V. Conclusion

We have presented an improved multi-phase model to simulate contact line problems with SPH. We simply modified the classical color-index gradient calculation to impose the correct stress boundary condition at the contact line and achieved a strong decrease of the spurious motion at the equilibrium state. We compared the spreading of a drop under gravity with analytical asymptotic solutions and found good agreement.

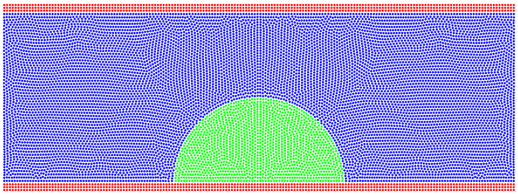

Fig. 8. Particle snapshot of the drop spreading at Eo=0.

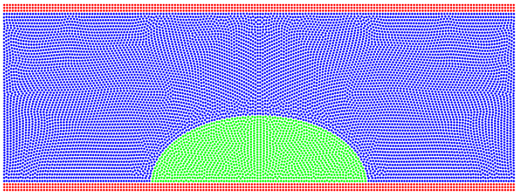

Fig. 9. Particle snapshot of the drop spreading at Eo=2.

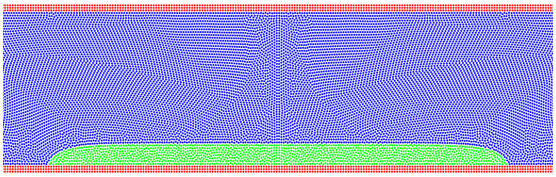

Fig. 10. Particle snapshot of the drop spreading at Eo=20.

Currently, we study the capabilities of this method to handle complex moving contact lines where the classical no-slip condition as wall boundary condition is violated and apply our method to realistic problems that are dominated by contact-line dynamics as e.g. drop impacts on walls.

REFERENCES

[1] JU Brackbill, DB Kothe, and C Zemach. A continuum method for modeling surface tension. *Journal of Computational Physics*, 100(2):335–354, 1992.

[2] A.K. Das and P.K. Das. Equilibrium shape and contact angle of sessile drops of different volumesComputation by SPH and its further improvement by DI. *Chemical Engineering Science*, 65(13):4027–4037, July 2010.

[3] Jean-Baptiste Dupont and Dominique Legendre. Numerical simulation of static and sliding drop with contact angle hysteresis. *Journal of Computational Physics*, 229(7):2453–2478, April 2010.

[4] X Hu and N Adams. A multi-phase SPH method for macroscopic and mesoscopic flows. *Journal of Computational Physics*, 213(2):844–861, April 2006.

[5] J J Monaghan. Smoothed particle hydrodynamics. *Reports on Progress in Physics*, 68(8):1703–1759, August 2005.

[6] Joseph P. Morris. Simulating surface tension with smoothed particle hydrodynamics. *International Journal for Numerical Methods in Fluids*, 33(3):333–353, June 2000.

[7] Joseph P. Morris, Patrick J. Fox, and Yi Zhu. Modeling Low Reynolds Number Incompressible Flows Using SPH. *Journal of Computational Physics*, 136(1):214–226, September 1997.

[8] S Nugent and Ha Posch. Liquid drops and surface tension with smoothed particle applied mechanics. *Physical review. E*, 62(4 Pt A):4968–75, October 2000.

[9] Alexandre Tartakovsky and Paul Meakin. Modeling of surface tension and contact angles with smoothed particle hydrodynamics. *Physical Review E*, 72(2):1–9, August 2005.